Advanced Steel Construction – Vol. 22 No. 4 (2026) 418–431
DOI:10.18057/IJASC.2026.22.4.6

MOMENT CAPACITY PREDICTION OF HIGH STRENGTH STEEL (HSS)-ECC COMPOSITE BEAMS USING MACHINE LEARNING MODELS

Cong-Luyen Nguyen * and Binh-Nam Nguyen

The University of Danang - University of Science and Technology, Danang, Vietnam

* *(Corresponding author: E-mail: ncluyen@dut.udn.vn)*

A B S T R A C T

The demand for high-performance structures has led to the development of composite beams made of High Strength Steel (HSS) I-section and Engineered Cementitious Composites (ECC) slab connected through headed shear studs, which could enhance both ductility and flexural capacity compared to conventional counterpart. Accurate prediction of flexural strength in HSS-ECC composite beams is crucial for optimal design and safety. This study presents a machine learning approach, including five machine learning (ML) models (i.e., Extreme Gradient Boosting (XGBoost), Artificial Neural Network (ANN), Support Vector Regression (SVR), Categorical Boosting (CatBoost), and Random Forest (RF)) to predict the flexural capacity of HSS-ECC composite beams. A total of 135 composite beam data were compiled and utilized for training and validating the machine learning models. By using performance metrics, it is indicate that all of the employed ML models showed excellent predicted performance, among which the SVR model exhibits superior predictive accuracy by achieving the lowest prediction errors (MAE, MAPE, and RMSE) together with the highest coefficient of determination (R^2 = 0.99), indicating superior generalization ability. This offers a viable alternative to traditional analytical approaches for predicting structural engineering.

A R T I C L E   H I S T O R Y

Received: 5 January 2026
Revised: 16 February 2026
Accepted: 13 March 2026

K E Y W O R D S

HSS-ECC composite beams;
Moment capacity;
Machine learning;
Extreme Gradient Boosting (XGBoost);
Artificial Neural Network (ANN);
Support Vector Regression (SVR)

1. Introduction

The construction industry continuously pursues structural materials that can provide higher strength and ductility while simultaneously reducing self-weight and overall cost. High-strength steel (HSS), owing to its superior mechanical performance, has been increasingly adopted in modern steel construction. In conventional composite beam systems, a normal-strength concrete (NSC) slab is linked with normal strength steel (NSS) I-section by means of headed shear studs. However, when HSS replaces normal-strength steel in these systems, significant strain incompatibility can arise between the employed materials (i.e., HSS and NSC). This mismatch often leads to unsafe structural behavior, characterized by brittle concrete crushing at ultimate load levels [1–7]. This challenge has motivated researchers worldwide to explore alternative materials capable of working compatibly with HSS in composite beams subjected to sagging moments. Engineered Cementitious Composites (ECC) have recently appeared as a potential substitute for the NSC. Originally developed by Victor Li several decades ago [8–11], ECC has soon demonstrated an advanced cement-based material due to its superior mechanical properties. Unlike ordinary concrete, ECC exhibits high strain capacity in both tension and compression, accompanied by multiple fine cracking and effective crack-bridging behavior [12–17]. Experimental studies by the author [18] demonstrated that composite beams consisting of a HSS I-girder combined with an ECC slab (hereafter referred to as HSS–ECC composite beams) can achieve comparative flexural capacity and enhanced ductility compared to traditional composite beams constructed with NSS and NSC. To facilitate the practical adoption of this composite system in commercial steel structures, various analytical and numerical investigations, including parametric studies, have been carried out [19–20]. Nevertheless, traditional analytical and numerical methods frequently face difficulties in precisely representing the complex and strongly nonlinear response of HSS–ECC composite beams.

Recent advancements in machine learning (ML) have attracted great attention due to its ability to identify complex data patterns and construct accurate, generalizable predictive models for targeted applications [21].One of the primary advantages of computational intelligence techniques is their strong pattern-recognition capability, which is particularly valuable in engineering problems. Although many ML models function as black-box systems, they are highly effective at identifying intricate relationships within data. In structural engineering, ML approaches have been increasingly adopted to assist decision-making and to extract useful insights from large datasets. In contrast to conventional numerical simulations, ML methods learn directly from extensive experimental and numerical data, enabling reliable predictions with minimal manual intervention. Moreover, by efficiently exploiting existing data, these approaches can reduce computational cost, experimental effort, and the need for repetitive testing [22]. Among the diverse machine learning approaches, Artificial Neural Networks (ANNs) have been extensively utilized to estimate the mechanical response and performance of concrete and steel structural systems. Their strong capability to represent highly nonlinear relationships and to process multiple input parameters simultaneously makes them particularly well suited for complex civil engineering applications. As a result, ANNs have become one of the most commonly adopted techniques in structural engineering research. Numerous studies have demonstrated the effectiveness of ANN models in predicting different structural behaviors. Typical examples include the estimation of axial compressive strength of various column configurations [23–24], shear strength and deflection of FRP-reinforced concrete beams [25–26], bond performance between GFRP bars and concrete [27], load-carrying capacity of corroded steel beams [28], and shear resistance of perfobond strip connectors [29]. Overall, these investigations highlight the strong predictive capability of ANN-based models for evaluating the structural performance of reinforced concrete systems. In addition to ANN, other advanced machine learning techniques have also shown considerable potential. Extreme Gradient Boosting (XGBoost), for instance, has been effectively applied to predict the strength capacity of ECC-reinforced beams [30] and FRCM-strengthened RC beams [31], yielding highly accurate load capacity estimations. Support Vector Regression (SVR) has likewise received significant attention in beam capacity prediction studies. Ahmad et al. [32] found that SVR can accurately predict splice strength of unconfined beams among the examined models. Similar conclusions were reported by Yuvaraj et al. [33] for fracture behavior of ultra-high-strength concrete beams and by Pal et al. [34] for strength estimation of deep beams. More recently, ensemble learning methods have demonstrated promising performance in structural engineering applications. Ge et al. [19] employed the Random Forest (RF) algorithm to estimate the flexural capacity of hybrid reinforced ECC–concrete composite beams, obtaining satisfactory predictive results. Taffese et al. [35] compared Categorical Boosting (CatBoost) with several ensemble models for predicting the flexural capacity of reinforced ultra-high-performance concrete (UHPC) beams and reported that CatBoost outperformed the other approaches across multiple evaluation metrics. Consistent findings were presented by Ye et al. [36], who confirmed the superior predictive accuracy of CatBoost in estimating the shear capacity of beams constructing using UHPC.

Despite the proven structural advantages of HSS–ECC composite beams, ML techniques' application for predicting their flexural capacity remains largely unexplored. Existing ML-based studies on composite beams are limited and focus on different performance aspects. For example, Oliveira et al. [37] predicted strength of steel–concrete composite beams subjected to lateral distortional buckling by employing ANN, Support Vector Machines (SVM), XGBoost, and RF models. The authors stated that all employed models appeared high accuracy (R^2 > 0.9) with XGBoost showing the best performance. Zhang et al. [38] applied ML models to field measurement data to predict temperature distributions in steel-concrete composite beams during hot asphalt paving. However, no prior research has investigated ML-driven prediction of flexural capacity for HSS–ECC composite beams. To address this gap, the present study evaluates five ML models, including XGBoost, ANN, SVR, CatBoost, and RF, for predicting the flexural capacity of HSS-ECC composite beams. Based on the data of 135 samples with eight input features selected, the above-mentioned ML models are assessed and evaluated. The findings of this study could provide a systematic comparison of selected ML models for predicting the flexural capacity of composite beams employing HSS and ECC, as well as evaluate their robustness for structural engineering applications.

2. Proposed methodology

2.1. Dataset

Due to the limited experimental data on moment capacity of HSS-ECC composite beams, this study collected data obtained from numerical analysis and a parametric study of 132 HSS-ECC composite beam models that have been reported in Refs. [19-20], in accordance with data of 3 HSS-ECC composite beams that have been experimentally conducted and presented in Ref. [18]. Those numerical results were obtained from a numerical model that was successfully verified against experimental data and deemed a reliable tool for simulating the structural performance and flexural capacity of composite beams constructing with HSS girder and ECC slab [18]. Although the numerical model was validated against experimental data [18], it should be emphasized that the present database is dominated by numerically generated samples (132 out of 135). Accordingly, the trained ML models mainly learn the response surface of the validated numerical model, and the reported high accuracy should be interpreted primarily as interpolation capability within the numerical parameter space rather than comprehensive experimental verification. Important real-world uncertainties (e.g., material variability, fabrication tolerances, residual stresses, boundary-condition imperfections, and environmental effects) are not fully represented in numerically generated data. Therefore, expanding the database with independent experiments/field data is recommended in future work. There have been eight input parameters that can influence the flexural capacity of HSS-ECC composite beams, including the beam's geometric dimensions (i.e., ECC slab width (b_{eff}), ECC slab thickness (t_c), HSS section height (h_a), HSS web thickness (t_w), HSS flange thickness (t_f)), material properties of components employed in the composite beams (i.e., ECC compressive strength (f'_c), HSS yielding strength (f_y)), and spacing of shear studs (s_d) which represents the shear connection degree in the beam. The explanation of the beam's geometric dimensions is shown in Fig. 1 and Table 1. It is worth noting that the headed shear stud used in studies of the authors [18-20] had a 19 mm shank diameter and a 100 mm height. A slab with profile steel sheeting with a trough height of 55 mm was employed in these studies [18-20]. The distributed values information of the input features is shown in Table 2 and Fig. 2. In Table 2, the minimum, maximum, and average values of the input parameters are presented as V_{min}, $V_{max,}$ and Ave., respectively. SD and COV stand for the standard deviation and coefficient of variation of the input values, respectively. The dataset of input values is tabulated in detail in the Appendix.

From the Kernel curves shown in Fig. 2, it is seen that the input values for ECC compressive strength f'_c vary between 40 and 70 MPa, and HSS yielding strength f_y is distributed between 690 and 960 MPa. The distribution of ECC slab width (b_{eff}) is between 600 and 1400 mm, while ECC slab thickness (t_c) values vary between 140 and 200 mm. HSS section height (h_a) ranges from 180 to 280 mm, centered around 230 mm. HSS web thickness (t_w) is distributed between 6 and 10 mm, while HSS flange thickness (t_f) varies from 8 to 12 mm, and shear studs spacing is distributed from 75 mm to 200 mm. The output values of moment capacity (M_u) were obtained by analysing a validated numerical model of HSS-ECC composite beams subjected to four-point bending configuration. The values of M_u range from 334.65 to 1070.08 kNm. Consequently, the applicability of the developed ML models is expected to be the highest for beams consistent with the data-generation setup (i.e., four-point bending) and for input variables within the ranges reported in Table 2. Data used outside these ranges and configurations constitutes extrapolation and may lead to increased prediction uncertainty.

Fig. 3 presents the Spearman correlation matrix of the input variables, which depicts the level of association among the selected features. The correlation coefficient varies between −1 and +1, where its absolute value reflects the strength of the relationship, and its sign indicates whether the association is positive or negative. A positive coefficient reflects a direct relationship between two variables, whereas a value close to zero implies little to no linear correlation. Conversely, a negative correlation coefficient signifies an opposite trend between variables, implying that higher values of one parameter are linked to lower values of the dependent variable. As observed in Fig. 3, all input features exhibit weak correlations, with correlation coefficients of relatively small magnitude. This suggests that no strong linear dependency exists among the input variables, indicating a low risk of multicollinearity and implying that each feature contributes independent information to the model.

Table 1
Explanation of input parameters

Component	Parameter	Explanation	Unit
ECC slab	f'_c	Compressive strength of ECC	MPa
	b_{eff}	ECC slab width	mm
	t_c	ECC slab thickness	mm
HSS I-section	f_y	Yield strength of HSS	MPa
	h_a	HSS I-section height	mm
	t_f	HSS I-section flange thickness	mm
	t_w	HSS I-section web thickness	mm
Shear studs	s_d	Shear studs spacing	mm

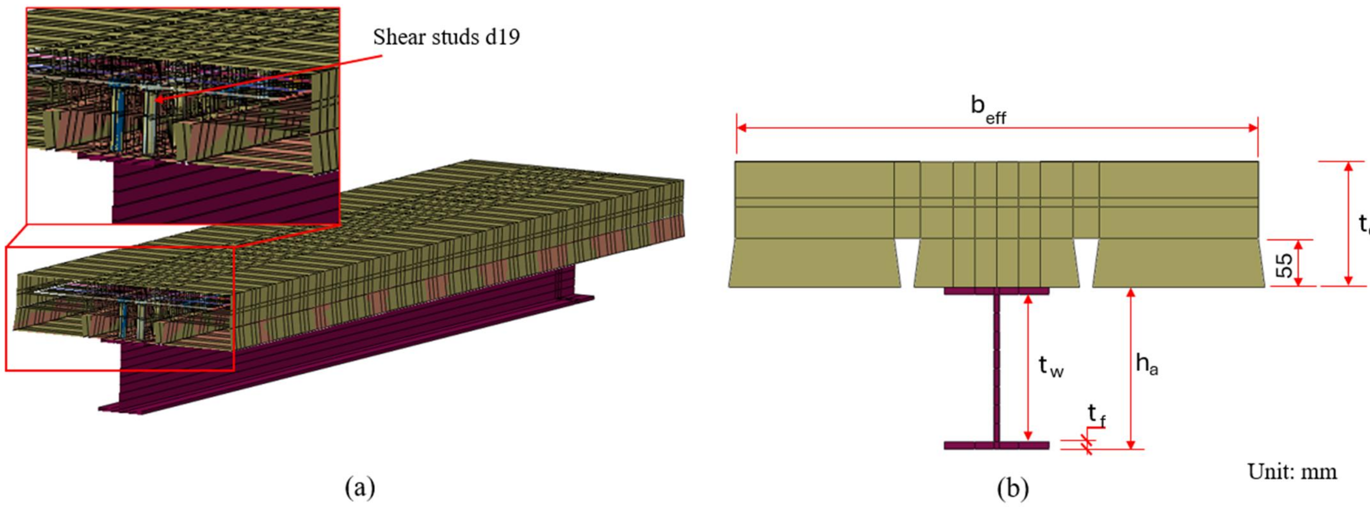

Fig. 1 Composite beam geometry: (a) Beam configuration; (b) Beam cross-section

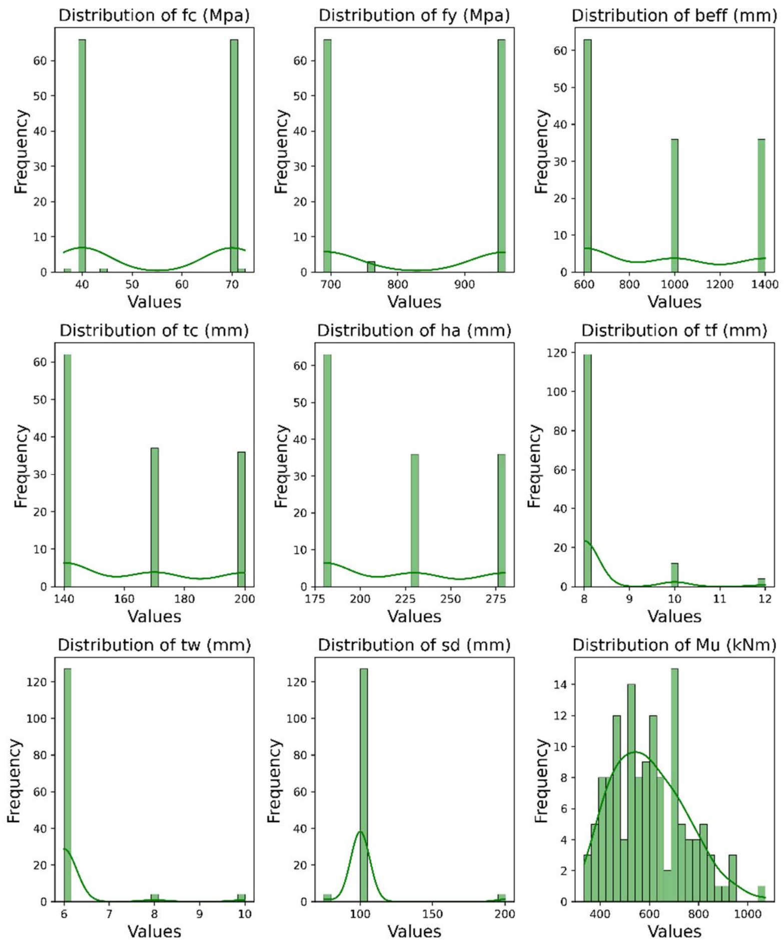

Fig. 2 Statistical distribution of input parameters

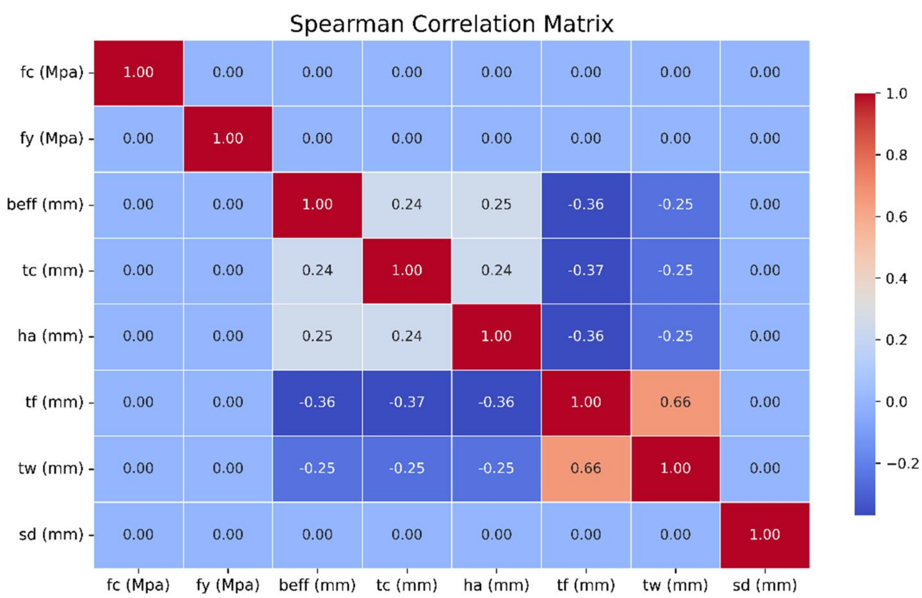

Fig. 3. Input feature Spearman correlation matrix

2.2. Preparation of the dataset

Preparing the dataset is a vital step in machine learning algorithms. It requires transforming all input and output parameters into a uniform dataset format. Converting raw data into a standardized range, such as from zero to 1, is referred to as normalization/standardization. By removing units through normalization/standardization, machine learning models can interpret the data more effectively. Normalization/standardization not only enhances data interpretability but also improves the model's accuracy, generalization, and learning performance. In this study, the dataset was normalized within the range of 0 to 1 using the following equation:

$$V' = \frac{V - V_{\max}}{V_{\max} - V_{\min}} \tag{1}$$

where V is the original value, V' is the normalised value (scaled between 0 and 1), V_{min} and V_{max} are the minimum and maximum values of the dataset. After standardizing, the data was separated into training and testing phases, with 80% utilized for training and the rest for testing the model.

Table 2
Statistical information of the input parameters

Parameter	Data type	V_{min}	V_{max}	Ave.	SD	CoV
f'_c (MPa)	Input	70	40	55.0	15.06	0.27
f_y (MPa)	Input	690	960	825.0	135.51	0.16
b_{eff} (mm)	Input	600	1400	927.3	334.55	0.36
t_c (mm)	Input	140	200	164.6	25.09	0.15
h_a (mm)	Input	180	280	220.9	41.82	0.19
t_f (mm)	Input	8	12	8.3	0.87	0.11
t_w (mm)	Input	6	10	6.2	0.76	0.12
s_d (mm)	Input	75	200	102.2	17.66	0.17
M_u (kNm)	Output	334.7	1070.1	596.7	149.3	0.25

2.3. Evaluation metrics

The performance of the developed ML models was assessed using several statistical metrics, namely the Coefficient of Determination (R^2), Root Mean Square Error (RMSE), Mean Absolute Error (MAE), and Mean Absolute Percentage Error (MAPE). These indicators collectively evaluate the accuracy and reliability of the models in predicting the flexural strength of HSS–ECC composite beams. Lower RMSE, MAE, and MAPE values indicate better predictive precision, while an R^2 value approaching 1 signifies strong consistency between predicted and actual results.While MAE, RMSE, MAPE, and R^2 are standard measures of predictive accuracy, their significance in structural engineering depends on how prediction errors affect safety, serviceability, and reliability. MAE reflects the average deviation between predicted and actual structural capacity; a low MAE reduces the risk of systematic bias, where underestimation leads to conservative and costly designs and overestimation may compromise safety. RMSE, by penalizing larger errors, is particularly relevant for structural safety, as occasional large deviations can control failure in critical members; a low RMSE indicates that such extreme errors are unlikely. MAPE expresses errors in relative terms, enabling practical interpretation; values on the order of 5–10% are generally acceptable for preliminary design and parametric studies, as they are typically smaller than the safety margins inherent in design codes, whereas higher values limit direct design applicability. R^2 indicates how well the model captures overall trends and parameter influences, which is valuable for optimization and sensitivity analysis, but it cannot alone ensure safe predictions and must be considered alongside absolute error metrics. Overall, these metrics suggest that the proposed models are best suited as decision-support or rapid prediction tools rather than direct substitutes for code-based design equations; with conservative bias or additional safety factors. They can aid preliminary design and comparative studies, while final design applications would require further experimental calibration and reliability assessment.

These metrics are expressed as in Eqs. 2–5, where $y, \hat{y}, \bar{y}$ denote the actual, predicted, and mean values of the dataset, respectively, whereas n represents the number of observations.

$$R^2 = 1 - \sum_{i=1}^{n} \frac{(\hat{y} - y_i)^2}{(\bar{y} - y_i)^2} \tag{2}$$

$$RMSE = \sqrt{\frac{1}{n}\sum_{i=1}^{n}(y_i - \hat{y})^2} \tag{3}$$

$$MAE = \frac{1}{n}\sum_{i=1}^{n}\left|\hat{y} - y_i\right| \tag{4}$$

$$MAPE = \frac{1}{n}\sum_{i=1}^{n}\left|\frac{y_i - \hat{y}}{y_i}\right| \tag{5}$$

3. Prediction approaches

This section describes the development of interpretable machine learning models, including SVR, XGBoost, ANN, RF, and CatBoost, and evaluates their predictive performance. The general framework of the proposed models is depicted in Fig. 4. The model development procedure comprises database construction, data preprocessing, model training, and optimization of hyperparameters.

3.1. ML prediction models

The structure of ML models is illustrated in Fig. 5, and the details are presented in the following sections.

3.1.1. Artificial Neural Network (ANN)

An Artificial Neural Network (ANN), also referred to as a Multilayer Perceptron (MLP), is a data-driven model inspired by the structure of the human brain. It comprises interconnected neurons arranged in an input layer, one or more hidden layers, and an output layer. Each connection carries a weight that is iteratively adjusted during training to reduce prediction error. The input layer represents the selected variables, the hidden layers capture complex nonlinear relationships, and the output layer (typically a single neuron) provides the predicted flexural capacity. In this study, the ANN architecture was optimized through hyperparameter tuning, including the number of hidden layers, neurons per layer, learning rate, and activation functions. The model was trained using backpropagation with Mean Squared Error (MSE) as the loss function, while early stopping and dropout were applied to improve generalization and mitigate overfitting.

3.1.2. Support Regression Vector (SVR)

Support Vector Regression (SVR), an extension of Support Vector Machines (SVM), is specifically formulated to model and predict continuous response variables. Rather than directly minimizing the prediction error, SVR aims to determine a regression function that lies within a specified tolerance margin (ε) around the training data. Errors within this margin are disregarded, while deviations exceeding it are penalized. The regression function can be expressed as in Eq. 6:

$$f(x) = w^T x + b \tag{6}$$

where w and b are parameters learned from the data. The goal is to keep the function as simple as possible while allowing deviations up to ε. A regularization parameter C controls how much the model tolerates errors outside this margin. Through the application of Kernel functions, including linear, polynomial, and radial basis function (RBF) kernels, SVR is capable of effectively capturing both linear and nonlinear relationships within the data.This makes it a flexible and reliable method for handling complex regression problems.

3.1.3. Extreme gradient boosting (XGBoost)

Extreme Gradient Boosting (XGBoost) is a powerful machine learning technique developed within the gradient boosting paradigm and is applicable to both regression and classification problems. The algorithm constructs an ensemble of weak predictive models (e.g., decision trees) through a sequential learning process. In this approach, each newly generated tree aims to minimize the residual errors produced by the preceding trees. The final prediction of the model is obtained by aggregating the outputs of all individual trees:

$$\hat{y}_i = \sum_{k=1}^{K} f_k(x_i) \qquad f_k \in F \tag{7}$$

where $\hat{y}_i$ denotes the predicted output for the i-th observation, K represents the total number of decision trees in the ensemble, and F defines the functional space of regression trees. The objective function in XGBoost integrates two main components: a loss term L, which quantifies the discrepancy between predicted and actual values, and a regularization term that penalizes model complexity to enhance generalization and reduce the risk of overfitting:

$$Obj = \sum_{i=1}^{n} L(y_i, \hat{y}_i) + \sum_{k=1}^{K} \Omega(f_k) \tag{8}$$

$$\Omega(f) = \gamma T + \frac{1}{2}\lambda \|w\|^2 \tag{9}$$

where T is the number of leaves in a tree, w is the leaf weights, γ and λ are the regularization parameters. By combining gradient descent with tree boosting and adding strong regularization, XGBoost achieves high accuracy, robustness, and efficiency, making it one of the most widely used algorithms in modern machine learning.

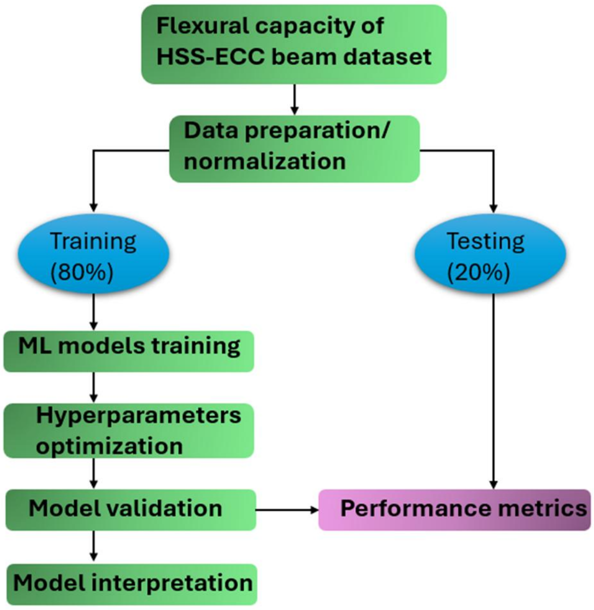

Fig. 4 Model development schemes

3.1.4. CatBoost

CatBoost is a gradient boosting–based machine learning algorithm introduced by Yandex, specifically designed to process categorical variables effectively without requiring complex preprocessing procedures. Similar to other boosting techniques, CatBoost constructs a sequence of decision trees in a stepwise fashion, where each successive tree is trained to reduce the residual errors generated by the preceding ensemble. The model output at iteration *t* can be formulated as:

$$F_t(x) = F_{t-1}(x) + \eta . h_t(x) \tag{10}$$

where $F_{t-1}(x)$ is the model from the previous iteration, $f_t(x)$ is the newly added weak learner (decision tree), and η is the learning rate. One of the primary strengths of CatBoost is its implementation of ordered boosting, which helps mitigate prediction shift during training. In addition, the algorithm employs an efficient target-based encoding scheme to process categorical features. Together, these mechanisms improve model robustness and generalization capability, making CatBoost especially effective for datasets with numerous categorical variables.

3.1.5. Random Forest (RF)

The Random Forest (RF) model is an ensemble learning method that constructs numerous decision trees and combines their outputs to improve accuracy and reduce overfitting. Each tree is trained on a bootstrap sample of the dataset, and at each split, a random subset of features is selected to increase model diversity. For regression problems, predictions are obtained by averaging the outputs of all trees, while for classification, the final decision is made by majority voting. The RF prediction can be expressed mathematically as:

$$\hat{y} = \frac{1}{T}\sum_{t=1}^{T} h_t(x) \tag{11}$$

where T is the trees' total number, $h_t(x)$ is the t-th decision tree prediction, and $\hat{y}$ is the final prediction. The randomness in feature selection and data sampling gives the model robustness and strong generalization ability.

3.2. Optimization of the models' hyperparameters

To enhance model accuracy, hyperparameters were optimized using a grid search approach with 6-fold cross-validation. Each parameter combination in the predefined grid was evaluated, and the set yielding the highest average validation score was selected as optimal. The process was implemented using the GridSearchCV function in the scikit-learn library. The key tuned hyperparameters for the five models are listed in Table 3, while all other settings remained at their default values.

Table 3
Hyperparameters used for ML models

Model	Parameters	Values
ANN	Layer 1 (Dense)	Units: 64, Activation: 'relu', Input: (X_train.shape[1],)
	Layer 2 (Dense)	Units: 64, Activation: 'relu'
	Layer 3 (Dense)	Units: 32, Activation: 'relu'
	Layer 4 (Output)	Units: 1
CatBoost Regressor	iterations	1500
	learning_rate	0.05
	depth	6
	l2_leaf_reg	5
	loss_function	RMSE'
	eval_metric	MAE'
	task_type	GPU'
	early_stopping_rounds	50
	verbose	100
	random_seed	42
RandomForest Regressor	n_estimators	1500
	criterion	squared_error'
	random_state	42
	bootstrap	TRUE
	max_leaf_nodes	20
	max_depth	10
	n_jobs	-1
SVR	kernel	rbf'
	C	1000
	epsilon	1
	gamma	0.2
XGB Regressor	base_score	0.5
	booster	gbtree'
	n_estimators	1100
	objective	reg:squarederror'
	max_depth	3
	learning_rate	0.03
	tree_method	gpu_hist'
	predictor	gpu_predictor'

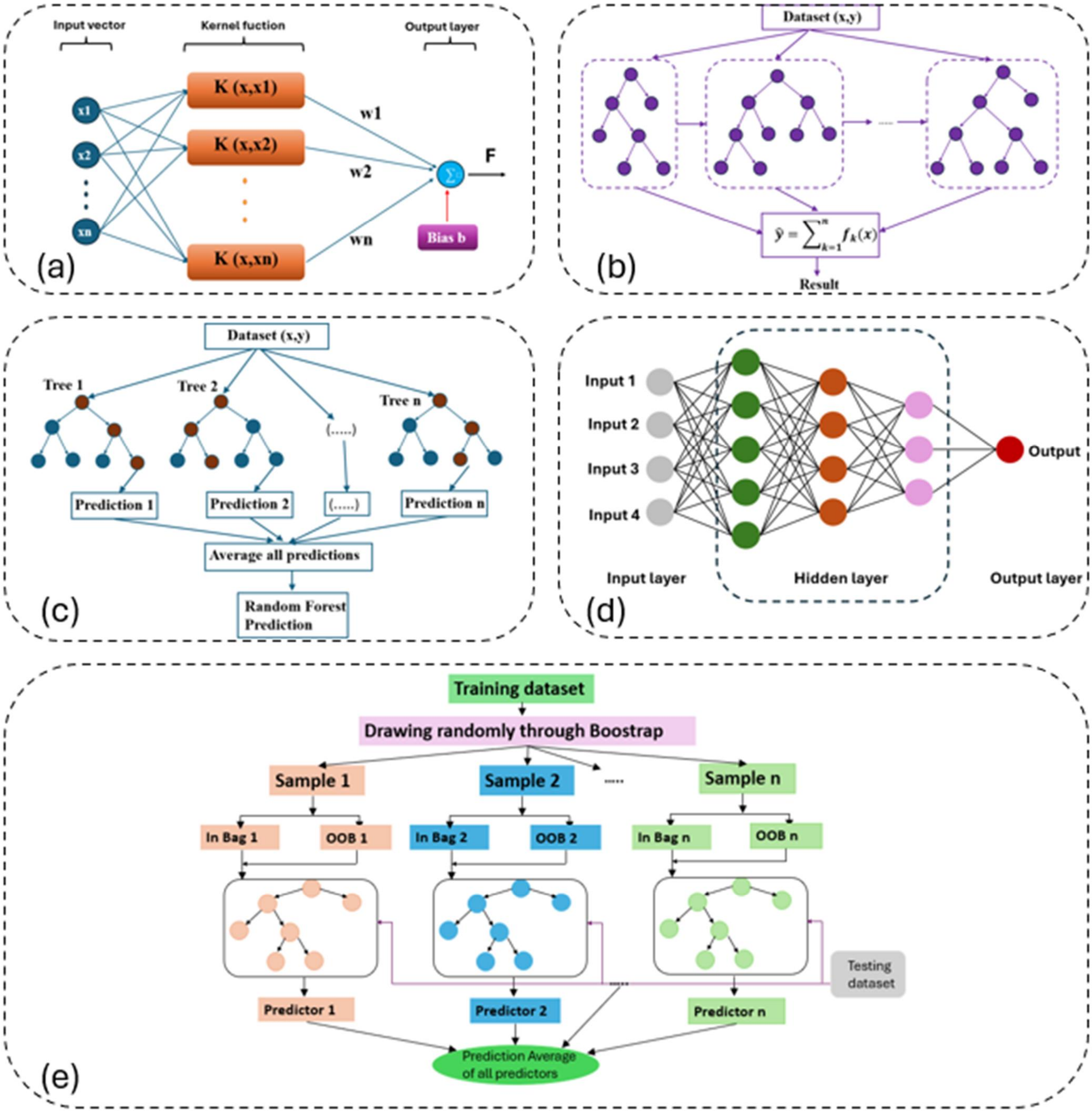

Fig. 5 Structures of ML models: a) ANN; b) SVR; c)XGBoost; d) CatBoost; e) RF

4. Analysis of predicted model performance

After determining the optimal hyperparameters for each algorithm, five machine learning models, including SVR, XGBoost, ANN, RF, and CatBoost, were developed using the training dataset. The predictive capability of these models was evaluated by comparing their outputs with the numerically obtained moment capacities of HSS–ECC composite beams. As depicted in Fig. 6, all five algorithms were able to reasonably estimate the flexural capacity of composite beams composed of HSS I-sections and ECC slabs. However, differences in predictive consistency were observed. The SVR and ANN models exhibited closer agreement with the reference values, while the RF model showed comparatively greater dispersion in its predictions. To further examine model performance, Fig. 7 illustrates scatter plots with linear regression fits between predicted and numerical results. In these plots, actual values are presented on the x-axis and predicted values on the y-axis. The solid diagonal line ($y = x$) represents perfect correspondence, whereas dashed lines corresponding to ±10% error bounds ($y = 0.9x$ and $y = 1.1x$) define acceptable prediction limits. A tighter clustering of points around the diagonal line indicates higher predictive accuracy and stability. Although all models captured the overall trend of the numerical data, the SVR model demonstrated the strongest alignment with the reference results. Predictions from SVR, ANN, CatBoost, and XGBoost largely fell within the acceptable error margins, whereas the RF model showed several data points exceeding the defined tolerance range, suggesting comparatively lower robustness. For quantitative assessment, statistical performance indicators, including RMSE, MAE, MAPE, and R^2, were computed for both training and testing datasets, as summarized in Table 4. In addition, radar and bar charts presented in Fig. 8 provide a visual comparison of these metrics across the five algorithms. These comparative analyses consistently indicate that SVR delivers the highest predictive accuracy and reliability in estimating the moment capacity of HSS–ECC composite beams.

A more detailed examination of Table 4 and Fig. 8 indicates that all developed machine learning models exhibit strong learning and predictive capabilities, with only minor differences attributable to the intrinsic mechanisms and limitations of each algorithm. High R^2 values were achieved for both training and testing datasets across all models, although the RF model recorded comparatively lower values. In terms of training performance, SVR and ANN demonstrated superior fitting ability, achieving the smallest error metrics (RMSE, MAE, and MAPE) on the training set. Meanwhile, XGBoost and CatBoost delivered closely comparable results across the evaluation criteria.

More notably, when assessing generalization performance on the testing dataset, SVR outperformed the remaining models. It produced the lowest prediction errors (MAE = 8.25, MAPE = 1.58, RMSE = 16.67) along with the highest coefficient of determination ($R^2 = 0.99$), indicating excellent agreement with the reference results. Overall, although all five models proved capable of estimating the moment capacity of HSS–ECC composite beams, SVR provided the most consistent balance between fitting accuracy and generalization performance. In contrast, the RF model showed comparatively weaker predictive capability, as reflected by its higher RMSE, MAE, and MAPE values and the lowest R^2 among the evaluated algorithms. The ANN model exhibited strong accuracy during training; however, a slight reduction in performance was observed on the testing dataset, suggesting minor generalization limitations. To further assess model robustness, Taylor diagrams were employed. These diagrams offer a comprehensive graphical comparison by simultaneously incorporating the correlation coefficient, centered root-mean-square error, and standard deviation into a unified geometric representation [39].

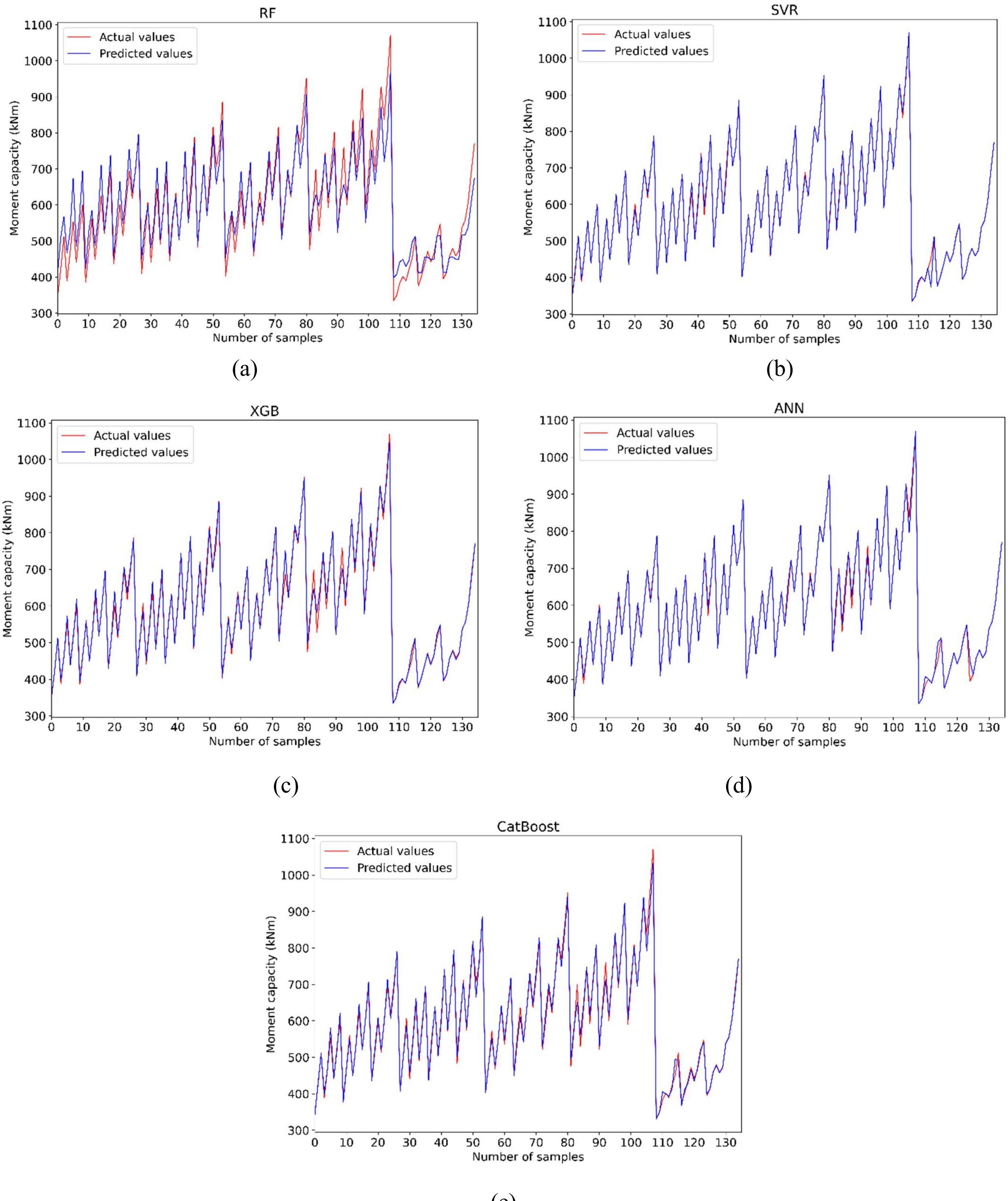

Fig. 6 Prediction values of ML models versus actual data: (a) RF; (b) SVR; (c) XGB; (d) ANN; (e) CatBoost

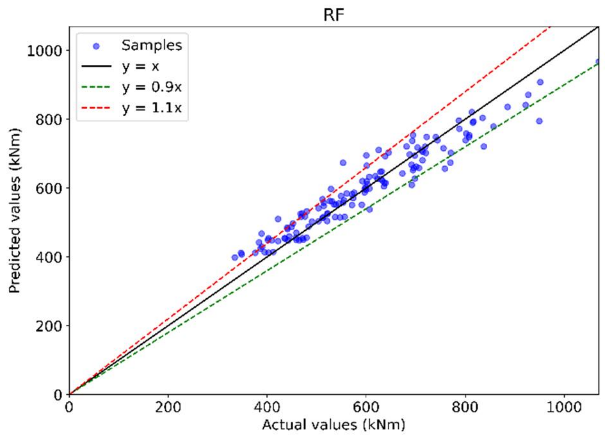

(a)

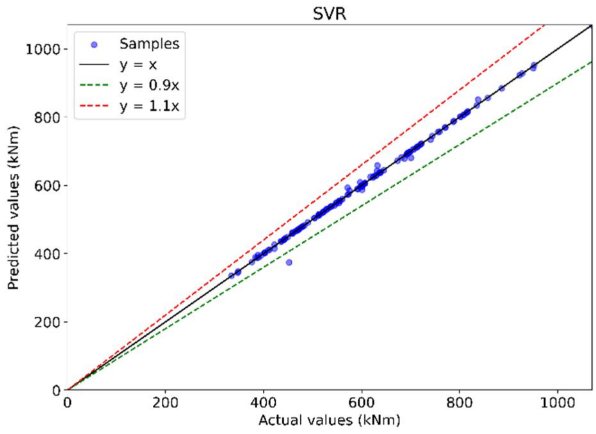

(b)

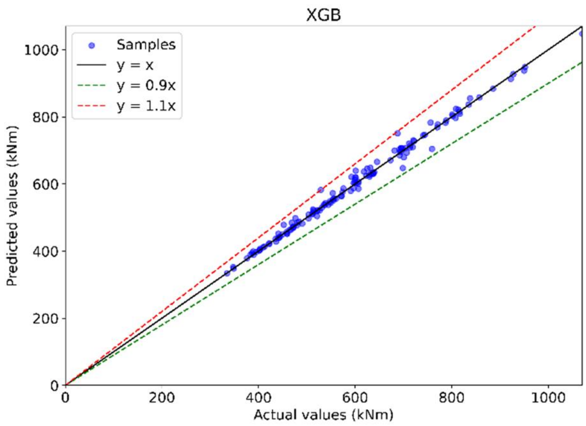

(c)

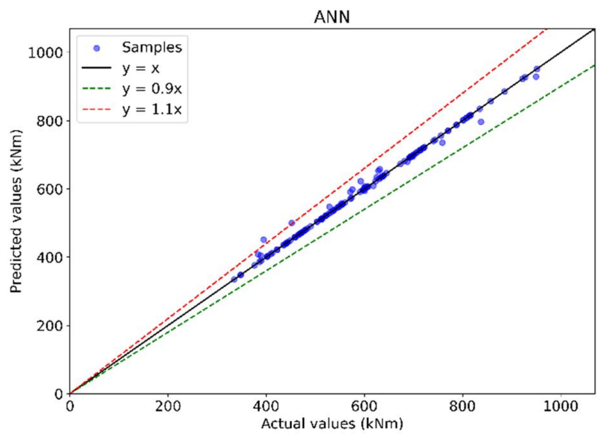

(d)

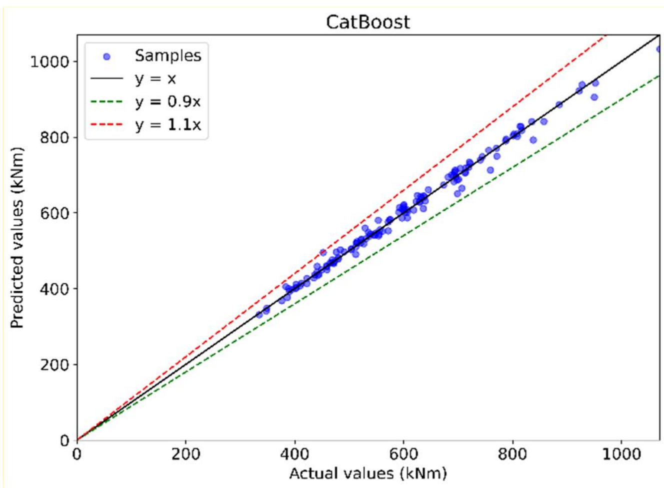

(e)

Fig. 7 Linear fitting plots of moment capacity of composite beams obtained by ML model (predicted value) and actual values: (a) RF; (b) SVR; (c) XGB; (d) ANN; (e) CatBoost

This approach allows performance comparisons by measuring how closely each model's results align with the actual data. Widely applied in assessing the behavior of composite materials, Taylor diagrams are particularly useful for analyzing predictive reliability. As depicted in Fig. 9, the purple dashed arcs represent centered RMSE, the radial axes indicate normalized standard deviation, and concentric curves display correlation coefficients. Both training and testing diagrams confirm that SVR attains higher correlation, reduced deviation, and smaller centered RMSE compared with other models, indicating that SVR provides the most accurate and stable learning as well as predictive outcomes.

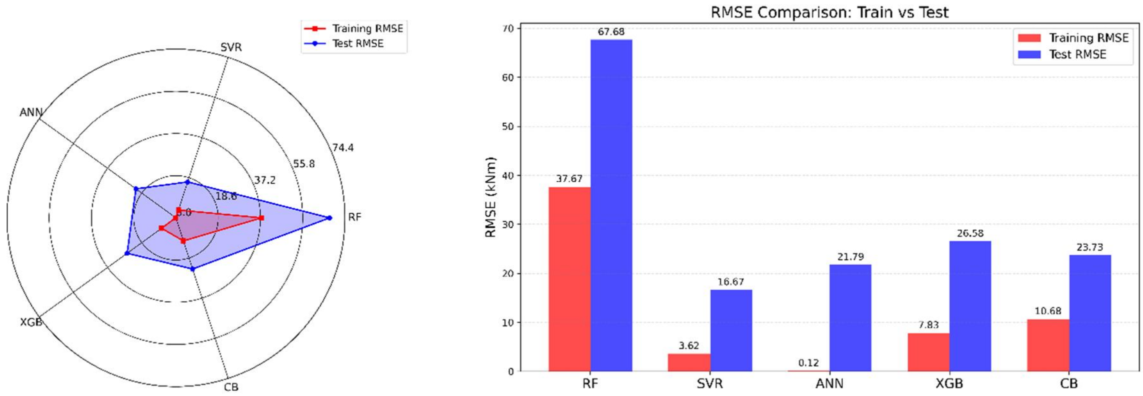

(a) RMSE

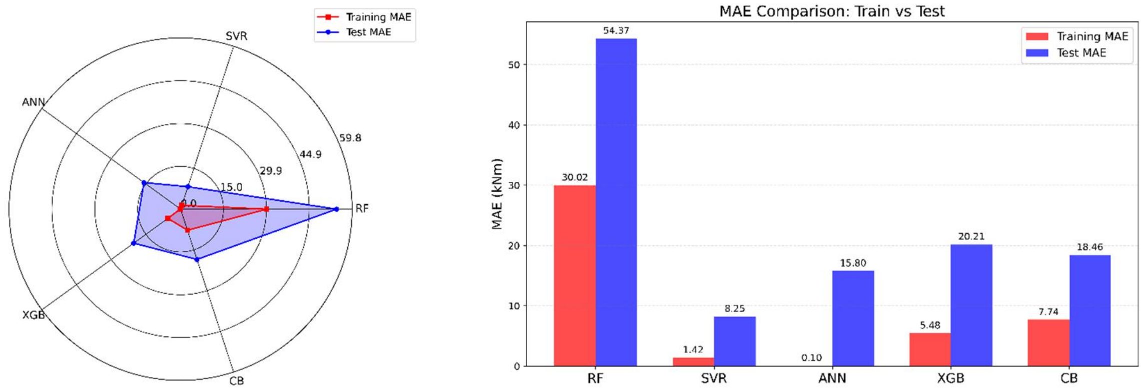

(b) MAE

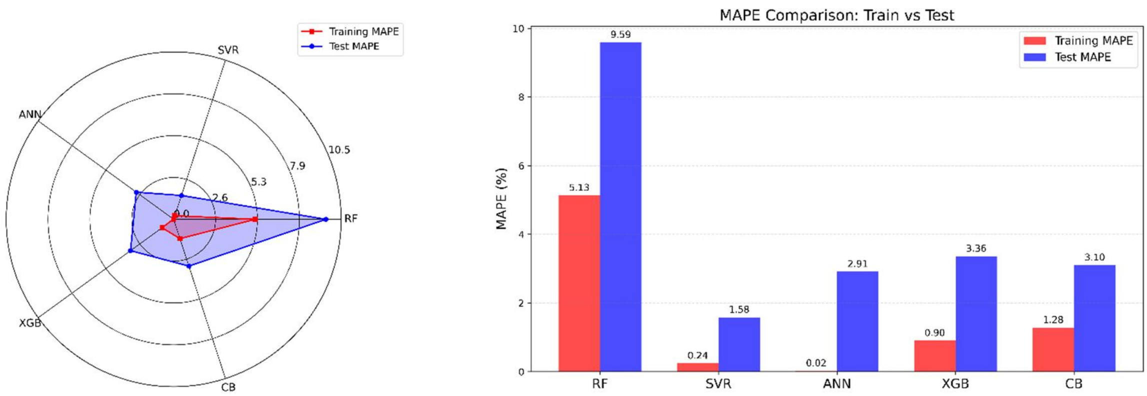

(c) MAPE

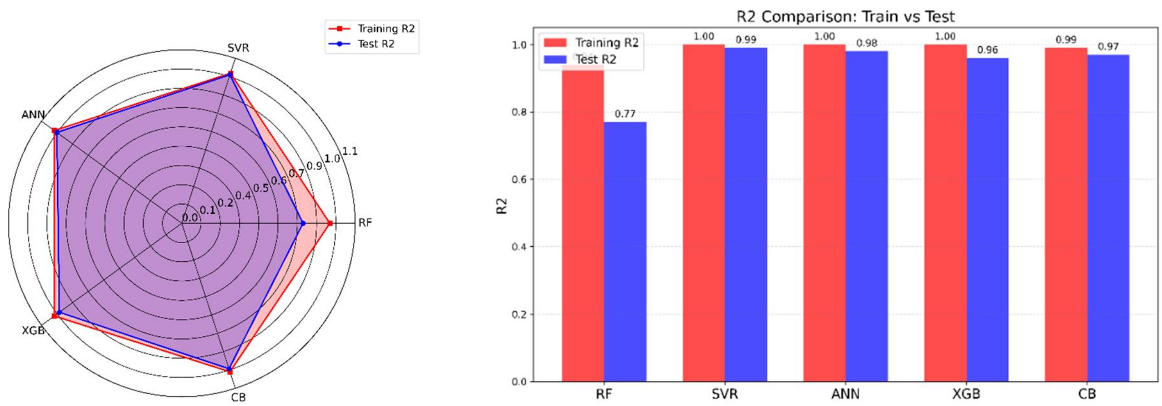

(d) R^2

Fig. 8 Evaluation metrics of ML models

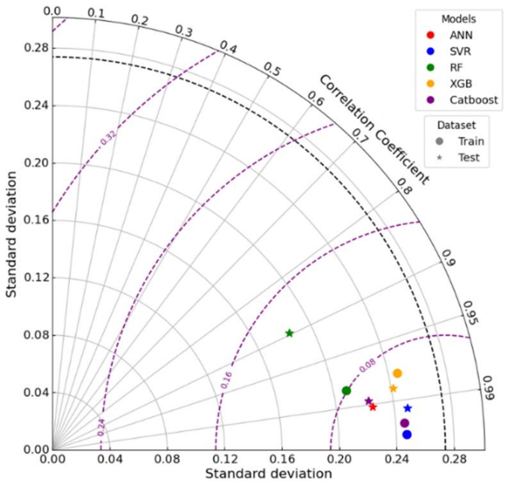

Fig. 9 Taylor diagram of ML models

Table 4
Evaluation metrics of ML models

Eva. Metr.	Dataset	RF	SVR	ANN	XGBoost	CatBoost
RMSE (kNm)	Train	33.67	3.62	0.12	7.83	10.68
	Test	67.68	16.67	21.79	26.58	23.73
MAE (kNm)	Train	30.02	1.42	0.10	5.48	7.74
	Test	54.37	8.25	15.08	20.21	18.46
MAPE (%)	Train	5.13	0.24	0.02	0.90	1.28
	Test	9.59	1.58	2.91	3.36	3.10
R^2	Train	0.94	1	1	1	0.99
	Test	0.77	0.99	0.98	0.96	0.97

5. Evaluation of input feature significance and correlation to the model output

The growing use of machine learning techniques in scientific research has highlighted the importance of interpretability approaches that can clarify the reasoning behind model predictions. Among the most commonly used interpretability frameworks is Shapley Additive Explanations (SHAP), which offers a robust, theoretically grounded approach to assessing the contribution of individual input variables. In contrast to conventional sensitivity analysis methods, SHAP evaluates not only the isolated effect of each feature but also its combined and interaction effects, thereby mitigating issues associated with multicollinearity. This approach determines the relative significance of each input variable by calculating its mean marginal effect over all possible feature subsets. The strength of each variable's influence is measured using the absolute SHAP values, where higher magnitudes correspond to a more significant impact on the model's prediction [40–42]. In this study, SHAP analysis was carried out on the SVR model since it demonstrated the most accurate model in the preceding evaluations. Fig. 10(a) presents a summary plot in which each data point represents an individual sample, and its horizontal position corresponds to the SHAP value of the associated feature. Positive SHAP values signify that a feature contributes to increasing the predicted moment capacity, whereas negative values indicate a contribution that reduces the predicted value. Feature values are represented using a color scale, where red denotes higher values, blue indicates lower values, and intermediate colors correspond to values near the mean. The spread and concentration of points along the horizontal axis reflect the relative influence of each variable. Fig. 10(b) presents an overall evaluation of feature significance using a bar chart derived from the mean absolute SHAP values computed over the entire dataset. The horizontal axis represents the average magnitude of the SHAP values, whereas the vertical axis displays the input variables ordered from the highest to the lowest level of influence. As can be seen from the results in Fig. 10, it is revealed that HSS section height (h_a), ECC slab thickness (t_c), ECC slab width (b_{eff}), ECC compressive strength (f'_c), and HSS yielding strength (f_y) play dominant roles in predicting moment capacity of the HSS-ECC composite beams, in which h_a is the most influential feature. In contrast, the HSS web thickness (t_w), HSS flange thickness (t_f), and shear studs spacing (s_d) marginally contribute to the model's predictions. From an engineering standpoint, the SHAP ranking is consistent with composite-beam mechanics. Increasing the HSS section height (h_a) primarily increases the internal lever arm between tensile and compressive resultants, leading to a pronounced increase in moment capacity. The ECC slab thickness (t_c) and effective width (b_{eff}) directly affect the compressive force that can be developed in the slab and its contribution to the composite section capacity. Material strengths (ECC compressive strength f'_c and HSS yield strength f_y) further scale these compressive and tensile resultants, respectively, and their effects become more pronounced when combined with larger lever arms and slab dimensions. The comparatively smaller SHAP contribution of shear stud spacing (s_d) should be interpreted within the scope of the dataset and modelling assumptions. It may reflect the limited variation range considered and/or idealizations in the numerical modelling of composite action. Therefore, while SHAP provides a useful "priority map" for flexural capacity improvement within the studied domain, variables with lower SHAP importance may still govern other design checks (e.g., shear connection design, local stability, constructability) and should not be disregarded.

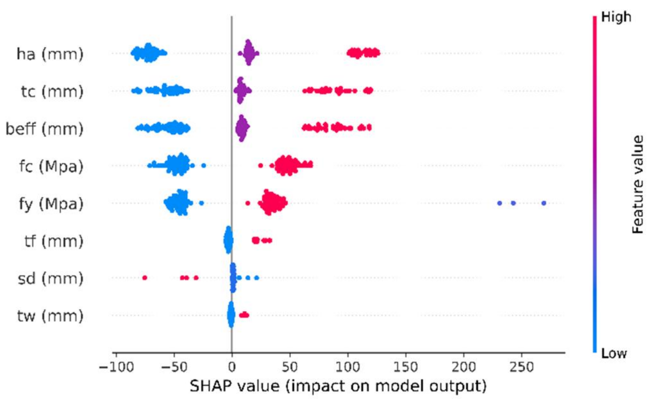

(a)

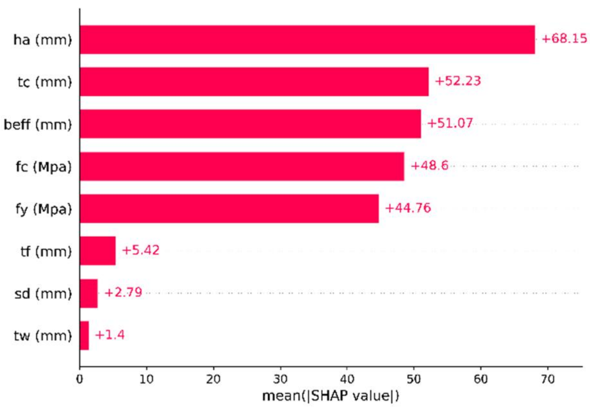

(b)

Fig. 10 SHAP plots of input features: (a) SHAP value; (b) mean SHAP value

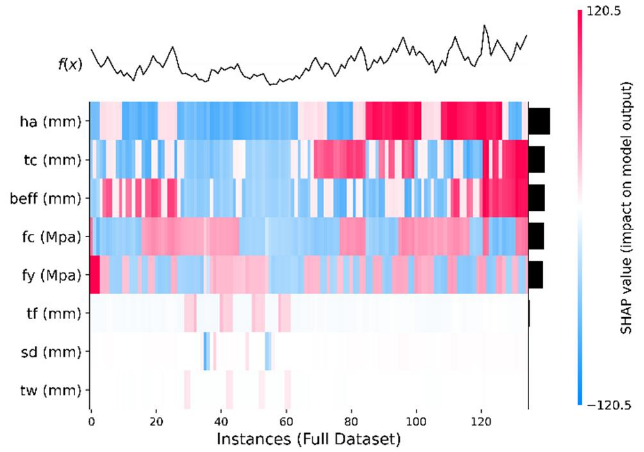

Fig. 11 SHAP heatmap of input features

In addition, SHAP values were further visualized using a clustered heatmap to enable a more integrated interpretation of feature contributions. In this representation, individual samples are arranged in the horizontal direction, while the corresponding predicted responses are shown in the vertical axis. The color intensity within the matrix denotes the SHAP value associated with each input variable, and hierarchical clustering is employed to group samples exhibiting similar contribution patterns. As illustrated in Fig. 11, the SHAP heatmap displays the predicted outputs above the matrix, a dashed gray line indicating the reference baseline, and a bar plot on the right summarizing the overall input features' importance. The variation of the prediction function f(x) across samples reflects the cumulative influence of SHAP values on the model output. The results consistently demonstrate that the HSS section height (h_a) exerts the strongest influence on moment capacity predictions, whereas HSS web thickness (t_w) and HSS flange thickness (t_f) and shear studs spacing (s_d) contribute the least. Taken together, the SHAP summary plots and the heatmap generated from the SVR model provide a clear and interpretable explanation of the relative significance of input parameters, enhancing insight into their effects on the flexural behavior of composite beams employing HSS and ECC.

6. Conclusions

This study systematically investigates the flexural capacity of HSS–ECC composite beams using five machine learning algorithms, namely Extreme Gradient Boosting (XGBoost), Support Vector Regression (SVR), Random Forest (RF), Artificial Neural Networks (ANN) and CatBoost. A database comprising 132 numerical samples data and 3 experimental data collected from the author's published studies was established. Eight influential input features were selected, preprocessed, and analyzed to develop robust predictive models. To improve interpretability and provide deeper insight into the prediction mechanism, the Shapley Additive Explanations (SHAP) method was employed to quantify the specific contribution of each input variable to the flexural capacity of HSS–ECC composite beams. The key findings derived from this analysis are summarized below:

1. The SVR and ANN algorithms demonstrate outstanding training performance, reflected by their minimal RMSE, MAE, and MAPE values. However, SVR further distinguishes itself on the testing dataset, achieving the lowest prediction errors (MAE, MAPE, and RMSE) together with the highest R^2 (R^2 = 0.99), indicating superior generalization ability. XGBoost and CatBoost yield similar and consistently stable results across all evaluation criteria, confirming their robustness. By comparison, the RF model delivers comparatively lower predictive accuracy, as evidenced by its higher error metrics and the smallest R^2 among the evaluated models.
2. Evaluation metrics comparisons reveal that the SVR model provides the most balanced performance in terms of accuracy and robustness. This observation is further supported by Taylor diagram analysis, which shows that the SVR model predictions are consistently closest to the actual results during both training and testing stages, confirming its superior learning capability.
3. SHAP-based interpretability analysis, including additive explanation plots and clustered heatmaps, identifies that the HSS section height (h_a), ECC slab thickness (t_c), effective ECC slab width (b_{eff}), ECC compressive strength (f'_c), and HSS yield strength (f_y) are the dominant parameters governing the predicted moment capacity of HSS–ECC composite beams, in which HSS section height (h_a) is the most influential feature. In contrast, the HSS web thickness (t_w), flange thickness (t_f), and shear studs spacing (s_d) exhibit a marginal influence on the model predictions.
4. The predictive reliability of the developed models is expected to be highest within the parameter ranges and loading configuration covered by the training data (Table 2; four-point bending setup). Application beyond these ranges constitutes extrapolation and may reduce accuracy. Therefore, the proposed ML models are recommended as decision-support tools for preliminary design and rapid assessment; further independent experimental datasets and reliability calibration are required before direct replacement of code-based design procedures.

References

[1] Uy B. and R. Sloane, "Behavior of composite tee beams constructed with high strength steel", Journal of Constructional Steel Research, 1: 203-204, 1998. https://doi.org/10.1016/S0143-974X(98)00126-6

[2] Zhao H. and Yuan Y., "Experimental studies on composite beams with high-strength steel and concrete", Steel and Composite Structures, 10(5): 373-383, 2010. https://doi.org/10.12989/scs.2010.10.5.373.

[3] Ban H. and Bradford M.A., "Flexural behaviour of composite beams with high strength steel", Engineering Structures, 56: 1130-1141, 2013. https://doi.org/10.1016/j.engstruct.2013.06.040.

[4] Shamass R. and Cashell K.A., "Behaviour of Composite Beams Made Using High Strength Steel", Structures, 12: 88-101, 2017. https://doi.org/10.1016/j.istruc.2017.08.005.

[5] Ban H., Bradford M. A., Uy B., and Liu X., "Available rotation capacity of composite beams with high strength materials under sagging moment", Journal of Constructional Steel Research, 118: 156-168, 2016. https://doi.org/10.1016/j.jcsr.2015.11.008.

[6] Ban H. and Bradford M.A., "Elastoplastic cross-sectional behavior of composite beams with high-strength steel: analytical modeling", Journal of Structural Engineering, 141(10): 04014236, 2015. https://doi.org/10.1061/(ASCE)ST.1943-541X.0001208.

[7] Nguyen C.-L. and Lee C.-K., "Experimental study of flexural behaviour of high strength steel (HSS) - Engineered Cementitious Composites (ECC) composite beam with profiled steel sheeting", ce/papers, 4: 781-786, 2021. https://doi.org/10.1002/cepa.1361.

[8] Li V. C., Mishra D. K., Naaman A. E., Wight J. K., LaFave J. M., Wu H. C., and Inada Y., "On the shear behavior of engineered cementitious composites", Advanced Cement Based Materials, 1(3), 142-149, 1994. DOI: https://doi.org/10.1016/1065-7355(94)90045-0.

[9] Li V. C., "On engineered cementitious composites (ECC) a review of the material and its applications", Journal of Advanced Concrete Technology, 1(3), 215-230, 2003.

[10] Li V. C., "Tailoring ECC for special attributes: A review", International Journal of Concrete Structures and Materials, 6(3), 135-144, 2012.

[11] Li V. C., Engineered cementitious composites (ECC): bendable concrete for sustainable and resilient infrastructure. Springer, 2019.

[12] Yu K., Wang Y., Yu J., and Xu S., "A strain-hardening cementitious composites with the tensile capacity up to 8%", Construction and Building Materials, 137, 410-419, 2017. DOI: https://doi.org/10.1016/j.conbuildmat.2017.01.060.

[13] Yu, K., Ding, Y., Liu, J. and Bai, Y. "Energy dissipation characteristics of all-grade polyethylene fiber-reinforced engineered cementitious composites (PE-ECC)", Cement and Concrete Composites, 106, 103459, 2020.

[14] Yu, K., Li, L., Yu, J., Wang, Y., Ye, J., and Xu, Q., "Direct tensile properties of engineered cementitious composites: A review", Construction and Building Materials, 165, 346-362, 2018.DOI: https://doi.org/10.1016/j.conbuildmat.2017.12.124.

[15] Meng, D., Lee, C. K., and Zhang, Y. X., "Flexural and shear behaviours of plain and reinforced polyvinyl alcohol-engineered cementitious composite beams", Engineering Structures, 151, 261-272, 2017. DOI: https://doi.org/10.1016/j.engstruct.2017.08.036

[16] Yu, K. Q., Dai, J. G., Lu, Z. D., and Poon, C. S., "Rate-dependent tensile properties of ultra-high performance engineered cementitious composites (UHP-ECC)", Cement and Concrete Composites, 93, 218-234, 2018.

[17] Yu, K., Zhu, H., Hou, M., and Li, V. C., "Self-healing of PE-fiber reinforced lightweight high-strength engineered cementitious composite", Cement and Concrete Composites, 123, 104209, 2021.

[18] Nguyen C. L. and Lee C.K. "Flexural behaviours of Engineered Cementitious Composites - High strength steel composite beams". Engineering Structures, 2021, 249. https://doi.org/10.1016/j.engstruct.2021.113324

[19] Nguyen C.-L., and Lee C.-K., "Development of analytical models for predicting the flexural behaviour of engineered cementitious composites-high strength steel composite beams", Advanced Steel Construction, 2023, 19(3): 197-208

[20] Mai A D, Lee C K, and Nguyen C L., "Flexural performance of composite beam with high-strength steel girder and ECC slab: A comprehensive parametric study", Res. Eng. Struct. Mater; 11(3): 1345-1367, 2025.

[21] Zhang, Tao, Danying Gao, and Chengcheng Xue. "Flexural strength prediction of concrete beams reinforced with hybrid FRP and steel bars based on machine learning", Structures. Vol. 65. Elsevier, 2024.

[22] Naser MZ. "An engineer's guide to explainable artificial intelligence and interpretable machine learning: navigating causality, forced goodness, and the false perception of inference", Autom Constr;129:103821, 2021.

[23] Raza Ali, El Ouni Mohamed Hechmi, Baili Jamel, and uz Zaman Khan Qaiser, "Datadriven analysis on axial strength of GFRP-NSC columns based on practical artificial neural network Tool", Compos Struct; 291:115598, 2022.

[24] Karimipour Arash, Mohebbi Najm Abad Javad, and Fasihihour Nazanin, "Predicting the load-carrying capacity of GFRP-reinforced concrete columns using ANN and evolutionary strategy", Compos Struct; 275:114470, 2021

[25] Naderpour H, Poursaeidi O, and Ahmadi M, "Shear resistance prediction of concrete beams reinforced by FRP bars using artificial neural networks", Measurement, 126:299–308, 2018.

[26] Nguyen Hoan D, Zhang Qianhui, Choi Eunsoo, and Duan Wenhui, "An improved deflection model for FRP RC beams using an artificial intelligence-based approach", Eng Struct ;219:110793, 2020.

[27] Golafshani EM, Rahai A, and Sebt MH, "Artificial neural network and genetic programming

for predicting the bond strength of GFRP bars in concrete", Mater Struct;48(5):1581–602, 2015.
[28] Sharifi Y., and Tohidi S., "Ultimate capacity assessment of web plate beams with pitting corrosion subjected to patch loading by artificial neural networks", Advanced Steel Construction, 10(3), 325-350, 2014.
[29] Nguyen M. H., and Phan H. N., "A Bayesian-Optimized Neural Network Model For Shear Capacity Of A Perfobond Strip Connector In Various Types Of Composite Structures", Advanced Steel Construction, 20(4), 376-384, 2024.
[30] Ge W., Zhang F., Wang Y., Ashour A., Luo L., Qiu L., and Cao D., "Machine learning predictions for bending capacity of ECC-concrete composite beams hybrid reinforced with steel and FRP bars", Case Studies in Construction Materials, 21, e03670, 2024.
[31] Kumar A., Arora H. C., and Nehdi M. L., "Data-driven framework with graphical user interface for predicting flexural behavior of FRCM strengthened RC beams", In Structures (Vol. 71, p. 107917). Elsevier, 2025.
[32] Ahmad M. S., Adnan S. M., Zaidi S., and Bhargava P., "A novel support vector regression (SVR) model for the prediction of splice strength of the unconfined beam specimens", Construction and building materials, 248, 118475, 2020.
[33] Yuvaraj P., Murthy A. R., Iyer N. R., Sekar S. K., and Samui P., "Support vector regression based models to predict fracture characteristics of high strength and ultra high strength concrete beams", Engineering fracture mechanics, 98, 29-43, 2013. .
[34] Pal M., and Deswal S, "Support vector regression based shear strength modelling of deep beams", Computers & Structures, 89(13-14), 1430-1439, 2011.
[35] Taffese W. Z., and Zhu Y., "Explainable machine learning for predicting flexural capacity of reinforced UHPC beams", Engineering Structures, 343, 121188, 2025.
[36] Ye M., Li L., Yoo D. Y., Li H., Zhou C., and Shao X., "Prediction of shear strength in UHPC beams using machine learning-based models and SHAP interpretation", Construction and Building Materials, 408, 133752, 2023.
[37] de Oliveira V. M., de Carvalho A. S., Rossi A., Hosseinpour M., Sharifi Y., and Martins C. H., "Data-driven design approach for the lateral-distortional buckling in steel-concrete composite cellular beams using machine learning models". In Structures (Vol. 61, p. 106018). Elsevier, 2024, March.
[38] Zhang Y., Chu Y., Zou J., and Yu C., "Machine learning prediction of steel–concrete composite beam temperatures during hot asphalt paving", Measurement, 242, 116257, 2025.
[39] Almustafa M. K., and Nehdi M. L., "Machine learning model for predicting structural response of RC slabs exposed to blast loading", Engineering Structures, 221, 111109, 2020.
[40] Haque M. A., Chen B., Kashem A., Qureshi T., and Ahmed A. A. M., "Hybrid intelligence models for compressive strength prediction of MPC composites and parametric analysis with SHAP algorithm", Materials Today Communications, 35, 105547, 2023.
[41] Lundberg S. M., and Lee S. I., "A unified approach to interpreting model predictions", Advances in neural information processing systems, 30, 2017.
[42] Ekanayake I. U., Meddage D. P. P., and Rathnayake U., "A novel approach to explain the black-box nature of machine learning in compressive strength predictions of concrete using Shapley additive explanations (SHAP)", Case Studies in Construction Materials, 16, e01059, 2022.

Appendix

No.	f_c (Mpa)	f_y (Mpa)	b_{eff} (mm)	t_c (mm)	h_a (mm)	t_f (mm)	t_w (mm)	s_d (mm)	M_u (kNm)
1	40	690	600	140	180	8	6	100	347.3
2	40	690	600	140	230	8	6	100	422.1
3	40	690	600	140	280	8	6	100	511.8
4	40	690	600	170	180	8	6	100	388.7
5	40	690	600	170	230	8	6	100	467.5
6	40	690	600	170	280	8	6	100	553.2
7	40	690	600	200	180	8	6	100	440.6
8	40	690	600	200	230	8	6	100	526.7
9	40	690	600	200	280	8	6	100	600.3
10	40	690	1000	140	180	8	6	100	386.4
11	40	690	1000	140	230	8	6	100	470.9
12	40	690	1000	140	280	8	6	100	560.6
13	40	690	1000	170	180	8	6	100	449.1
14	40	690	1000	170	230	8	6	100	530.7
15	40	690	1000	170	280	8	6	100	625.0
16	40	690	1000	200	180	8	6	100	521.0
17	40	690	1000	200	230	8	6	100	602.6
18	40	690	1000	200	280	8	6	100	692.9
19	40	690	1400	140	180	8	6	100	436.4
20	40	690	1400	140	230	8	6	100	514.1
21	40	690	1400	140	280	8	6	100	600.9
22	40	690	1400	170	180	8	6	100	514.1
23	40	690	1400	170	230	8	6	100	606.1
24	40	690	1400	170	280	8	6	100	694.6
25	40	690	1400	200	180	8	6	100	618.1
26	40	690	1400	200	230	8	6	100	698.1
27	40	690	1400	200	280	8	6	100	787.2
28	40	960	600	140	180	8	6	100	409.4
29	40	960	600	140	230	8	6	100	503.7
30	40	960	600	140	280	8	6	100	606.6
31	40	960	600	170	180	8	6	100	441.0
32	40	960	600	170	230	8	6	100	538.8
33	40	960	600	170	280	8	6	100	645.2
34	40	960	600	200	180	8	6	100	490.5
35	40	960	600	200	230	8	6	100	596.9
36	40	960	600	200	280	8	6	100	681.4
37	40	960	1000	140	180	8	6	100	444.5
38	40	960	1000	140	230	8	6	100	554.9

39	40	960	1000	140	280	8	6	100	632.5
40	40	960	1000	170	180	8	6	100	503.7
41	40	960	1000	170	230	8	6	100	596.9
42	40	960	1000	170	280	8	6	100	740.6
43	40	960	1000	200	180	8	6	100	571.6
44	40	960	1000	200	230	8	6	100	673.3
45	40	960	1000	200	280	8	6	100	788.3
46	40	960	1400	140	180	8	6	100	483.6
47	40	960	1400	140	230	8	6	100	599.2
48	40	960	1400	140	280	8	6	100	711.9
49	40	960	1400	170	180	8	6	100	573.9
50	40	960	1400	170	230	8	6	100	700.9
51	40	960	1400	170	280	8	6	100	816.5
52	40	960	1400	200	180	8	6	100	706.7
53	40	960	1400	200	230	8	6	100	756.1
54	40	960	1400	200	280	8	6	100	885.5
55	70	690	600	140	180	8	6	100	402.5
56	70	690	600	140	230	8	6	100	480.1
57	70	690	600	140	280	8	6	100	571.6
58	70	690	600	170	180	8	6	100	468.6
59	70	690	600	170	230	8	6	100	549.1
60	70	690	600	170	280	8	6	100	638.3
61	70	690	600	200	180	8	6	100	535.3
62	70	690	600	200	230	8	6	100	629.6
63	70	690	600	200	280	8	6	100	703.8
64	70	690	1000	140	180	8	6	100	459.0
65	70	690	1000	140	230	8	6	100	553.7
66	70	690	1000	140	280	8	6	100	636.0
67	70	690	1000	170	180	8	6	100	544.5
68	70	690	1000	170	230	8	6	100	628.5
69	70	690	1000	170	280	8	6	100	722.2
70	70	690	1000	200	180	8	6	100	636.5
71	70	690	1000	200	230	8	6	100	720.5
72	70	690	1000	200	280	8	6	100	815.4
73	70	690	1400	140	180	8	6	100	521.0
74	70	690	1400	140	230	8	6	100	599.7
75	70	690	1400	140	280	8	6	100	687.7
76	70	690	1400	170	180	8	6	100	622.7
77	70	690	1400	170	230	8	6	100	719.3
78	70	690	1400	170	280	8	6	100	813.6
79	70	690	1400	200	180	8	6	100	771.1
80	70	690	1400	200	230	8	6	100	857.3
81	70	690	1400	200	280	8	6	100	951.6
82	70	960	600	140	180	8	6	100	476.1
83	70	960	600	140	230	8	6	100	575.6
84	70	960	600	140	280	8	6	100	698.6
85	70	960	600	170	180	8	6	100	529.0
86	70	960	600	170	230	8	6	100	631.4
87	70	960	600	170	280	8	6	100	744.1
88	70	960	600	200	180	8	6	100	592.4
89	70	960	600	200	230	8	6	100	713.6
90	70	960	600	200	280	8	6	100	802.1
91	70	960	1000	140	180	8	6	100	522.3

92	70	960	1000	140	230	8	6	100	639.4
93	70	960	1000	140	280	8	6	100	759.0
94	70	960	1000	170	180	8	6	100	600.9
95	70	960	1000	170	230	8	6	100	714.2
96	70	960	1000	170	280	8	6	100	834.9
97	70	960	1000	200	180	8	6	100	691.7
98	70	960	1000	200	230	8	6	100	801
99	70	960	1000	200	280	8	6	100	922.3
100	70	960	1400	140	180	8	6	100	591.1
101	70	960	1400	140	230	8	6	100	694.6
102	70	960	1400	140	280	8	6	100	808.5
103	70	960	1400	170	180	8	6	100	695.8
104	70	960	1400	170	230	8	6	100	807.9
105	70	960	1400	170	280	8	6	100	927.5
106	70	960	1400	200	180	8	6	100	837.8
107	70	960	1400	200	230	8	6	100	949.9
108	70	960	1400	200	280	8	6	100	1070.1
109	40	690	600	140	180	8	6	200	334.7
110	40	690	600	140	180	8	6	75	348.5
111	70	690	600	140	180	8	6	200	383.5
112	70	690	600	140	180	8	6	75	401.4
113	40	960	600	140	180	8	6	200	389.9
114	40	960	600	140	180	8	6	75	422.1
115	70	960	600	140	180	8	6	200	452.0
116	70	960	600	140	180	8	6	75	511.8
117	40	690	600	140	180	10	6	100	376.1
118	40	690	600	140	180	12	6	100	402.5
119	70	690	600	140	180	10	6	100	435.3
120	70	690	600	140	180	12	6	100	471.5
121	40	960	600	140	180	10	6	100	442.2
122	40	960	600	140	180	12	6	100	464.6
123	70	960	600	140	180	10	6	100	512.9
124	70	960	600	140	180	12	6	100	547.4
125	40	690	600	140	180	10	8	100	395.0
126	40	690	600	140	180	10	10	100	412.3
127	70	690	600	140	180	10	8	100	458.3
128	70	690	600	140	180	10	10	100	479.6
129	40	960	600	140	180	10	8	100	458.9
130	40	960	600	140	180	10	10	100	472.7
131	70	960	600	140	180	10	8	100	537.1
132	70	960	600	140	180	10	10	100	556.6
133	36.34	759	600	140	180	8	6	100	607
134	44.5	759	600	170	180	8	6	100	692
135	72.6	759	600	140	180	8	6	100	770